$^{12}C(\gamma, p_{0+1})^{11}B$ cross section from 44 to 98 MeV

K. Mori,[1] P. D. Harty,[2,3] Y. Fujii,[1] O. Konno,[1] K. Maeda,[4] I. Nomura,[1] G. J. O'Keefe,[2] J. Ryckebusch,[5] T. Suda,[1,4]
T. Terasawa,[1] M. N. Thompson,[2] and Y. Torizuka[1]

[1]*Laboratory of Nuclear Science, Tohoku University, Sendai 982, Japan*
[2]*School of Physics, The University of Melbourne, Parkville 3052, Australia*
[3]*Department of Physics and Astronomy, University of Glasgow, Glasgow G12 8QQ, United Kingdom*
[4]*Department of Physics, Tohoku University, Sendai 980, Japan*
[5]*Laboratory for Nuclear Physics and Institute for Theoretical Physics, Proeftuinstraat 86, B-9000 Gent, Belgium*
(Received 16 January 1995)

The $^{12}C(\gamma, p_{0+1})^{11}B$ differential cross section has been measured for tagged-photon energies of $E_\gamma = 44$–98 MeV, at laboratory angles of $30°$, $45°$, $65°$, and $90°$. Comparison has been made with four different types of calculation. Results from similar calculations for the photoneutron channel have been compared to previously published $^{12}C(\gamma, n_{0+1})^{11}C$ data.

I. INTRODUCTION

In the region of photon energy between the giant dipole resonance and photopion threshold there has been considerable interest in recent years, in an attempt to resolve the reaction mechanism. In this energy regime, the relative importance of one-body and two-body effects in the photoabsorption process is unclear. Several models have been used to explain the data. These range from the direct knockout (DKO) of the interacting nucleon using the one-body current form of the impulse approximation, through the quasideuteron (QD) model, to more microscopic models which have attempted to take into account the detailed NN interaction. These models have met with varied success.

Direct knockout on a single bound nucleon is inhibited by the large momentum mismatch between the photon and outgoing nucleon. The high-momentum components in single-nucleon wave functions, calculated from shell-model potentials, are not large enough to account for measured (γ, p_0) cross sections [1–3]. This model gives an even poorer description of the (γ, n_0) cross sections, since direct knockout of a neutron is unlikely due to the relatively weak interaction of the photon with the neutron via its magnetic moment, or with the charge in the remaining $(A-1)$ residual nucleus [4].

A more phenomenological description of the (γ, p_0) cross section was given by the modified QD model [5]. This model was based on the original QD model of Levinger [6], which parametrizes the (γ, pn) cross section in terms of deuteron photodisintegration. In the modified form, one of the nucleons from the photodisintegration of the QD is reabsorbed into its original state in the nucleus, allowing a (γ, p_0) or (γ, n_0) reaction to take place [5]. This model leads naturally to similar magnitudes for (γ, p_0) and (γ, n_0) cross sections, which has been confirmed experimentally [7–9].

The failure of the DKO model, coupled with the relative success of the QD model, leads immediately to the question of the importance of two-body effects. The in-clusion of final-state interactions [10] and Δ-resonance effects [11] were two attempts at this. However it became clear that these effects by themselves could not account for the observed features of the (γ, p_0) and (γ, n_0) cross sections. More consistent approaches have now been made in more microscopic models [1–3,12] which include the effects due to meson-exchange currents (MEC), coupling to the collective properties of the target nucleus, and rescattering effects.

In order to provide constraints on the latest theoretical calculations available, accurate data are needed over a wide range of energies and angles. The early bremsstrahlung data of Matthews *et al.* [13] have been supplemented now by some tagged-photon measurements of the $^{12}C(\gamma, p_{0+1})^{11}B$ differential cross section [14–19], and proton-capture data on ^{11}B [20–22]. There is a need for further data however, since there are discrepancies [19] between the data sets that are much larger than the quoted systematic errors. It is also clear that the available data do not yet cover a sufficient range of energies and angles to constrain the theoretical calculations adequately.

In this paper, data are presented for the $^{12}C(\gamma, p_{0+1})^{11}B$ differential cross section at four angles and 13 photon energies, over the range from 44 to 98 MeV. This coverage of angles and photon energies, within the same experiment, provides a good test of theoretical predictions. In particular, comparison with the results of four theoretical calculations are presented in Sec. IV.

II. EXPERIMENT

The experiment was performed with the linac, pulsed-beam stretcher, and the tagged-photon facility at the Laboratory of Nuclear Science at Tohoku University. The experimental arrangement has been shown previously in Ref. [23], which also contains many details of the tagging spectrometer, electronics, and data acquisition system. The 130 MeV electron beam from the stretcher had a

duty factor of 80%, and an energy spread of 0.2%. These electrons produced bremsstrahlung from a thin gold foil, which had a thickness of 10^{-3} radiation lengths. The recoil electrons from the gold foil were momentum analyzed by the photon-tagging magnet and detected by an array of 32 electron detectors on the focal plane of the spectrometer. Each electron detector consisted of a 5 mm thickness of plastic scintillator, with width ranging from 13 to 31 mm, in order to provide a constant energy bin of $\Delta E_\gamma = 2.6$ MeV along the length of the focal plane.

The range of available tagged-photon energies was from 25 to 102 MeV, but below $E_\gamma = 44$ MeV the protons from the ^{12}C$(\gamma, p_{0+1})^{11}$B reaction were not all above the proton detector threshold of 20 MeV. The intensity of the tagged photons used in the experiment was $N_\gamma = 3 \times 10^6$ s^{-1}. Collimation of the photons provided a beam diameter of 40 mm at the target position, 1.5 m downstream from the tagging spectrometer. Sweep magnets were placed directly after the collimators to remove secondary electrons from the beam. The ratio of the number of tagged photons to the number of electron counts in the focal plane (the tagging efficiency) was measured at the target position using an 80 mm×100 mm×300 mm lead-glass Čerenkov detector placed at the target position. The measured tagging efficiency was 0.50±3%. This agrees with the result of a Monte Carlo calculation [23], which took into account effects due to multiple scattering, Møller scattering, collimation, and the bremsstrahlung angular distribution.

A natural graphite target of thickness 196 mg cm^{-2} was positioned at 45° with respect to the beam. Photoprotons from this target were detected by scintillation spectrometers positioned at four angles, $\theta_p = 30°$, 45°, 65°, and 90°. Each spectrometer consisted of two thin ΔE layers consisting of 1 mm thick plastic scintillator, in front of a 75 mm diameter by 50 mm thick NaI(Tl) detector as the total energy E counter. Timing coincidences between the electron focal-plane detectors and the proton detectors were recorded by 32 time-to-digital convertors (TDC's), one for each channel. The separate TDC's for each electron channel allowed events with multiple hits among the electron detectors to be processed without loss of information. The TDC's provided the necessary timing information for identification of regions of prompt and random coincidences, which were used in the analysis.

III. ANALYSIS AND RESULTS

In order to extract the ^{12}C$(\gamma, p_{0+1})^{11}$B differential cross section from the data, protons were separated cleanly from other charged particles by the use of scatter plots of ΔE vs E. Proton energies were determined with a resolution of ~1.5 MeV for 50 MeV protons, using the pulse-height information recorded from the E detectors, and taking into account energy loss of the protons in the ΔE layers, air, and target. Conversion of this information into missing-energy (E_m) spectra for each proton angle and photon-energy bin was performed using the following definition of E_m:

$$E_m = E_\gamma - E_p - E_r \, , \tag{1}$$

where E_γ is the photon energy, E_p is the proton kinetic energy, and E_r is the kinetic energy of the recoiling system calculated from the photon and proton momenta. For photon energies above 53 MeV the E_m spectra for neighboring photon-energy bins were combined, in order to improve the statistics.

The E_m spectra were subtracted for the background due to random coincidences with the tagger focal-plane detectors and background from protons not associated with the target. Some sample E_m spectra from this experiment were shown previously in Fig. 10 of Ref. [7]. The resolution of the E_m spectra was ~4 MeV full width at half maximum, so that photoproton reactions leading to the ground and first-excited states of ^{11}B could be resolved from reactions leaving ^{11}B at higher excitation.

Differential cross sections were deduced by integrating over the first peak in the E_m spectra and applying the formula:

$$\frac{d\sigma}{d\Omega} = \frac{N_{\mathrm{coinc}}}{\Delta \Omega N_e \eta N_C} \tag{2}$$

where N_{coinc} is the number of coincident events in the integrated peak, $\Delta \Omega$ is the solid angle subtended by each proton spectrometer, N_e is the total number of electron counts recorded at the focal plane, η is the tagging efficiency, and N_C is the effective number of ^{12}C nuclei per area of the target.

The results at the 4 center-of-mass (c.m.) angles are listed in Table I and shown in Fig. 1, compared to the other presently available data. For all data sets, only the statistical errors have been shown, except for the proton-capture data of Anghinolfi *et al.* [20] (diamonds), which have statistical and systematic errors combined. The systematic uncertainty for the present data is estimated to be ±10%. For the ^{12}C$(\gamma, p_{0+1})^{11}$B data sets of Matthews *et al.* [13] (open circles), McGeorge *et al.* [14] (squares), Springham *et al.* [16] (stars), Van Hoorebeke *et al.* [17] (asterisks), Harty *et al.* [19] (triangles), and proton-capture data of Höistad *et al.* [22] (open cross), the quoted systematic errors are 22%, 15%, 22%, 15%, 10%, and 8%, respectively. It can be seen that with the exception of a few points, there is generally agreement among the different data sets. One place where there are some discrepancies between data sets occurs at $\theta_{\mathrm{c.m.}} = 91°$ and $E_\gamma = 80$ MeV. This discrepancy was recently highlighted in Ref. [19].

The two proton-capture data sets have been transformed by detailed balance. Since these transformed data include only the ^{12}C$(\gamma, p_0)^{11}$B cross section, a scaling factor of 1.27 has been applied in order to allow comparison with the ^{12}C$(\gamma, p_{0+1})^{11}$B data sets. This factor was chosen after comparing data sets of ^{12}C$(\gamma, p_0)^{11}$B and ^{12}C$(\gamma, p_1)^{11}$B cross sections [13,16,17], at similar photon energies to those considered here.

IV. CROSS SECTION CALCULATIONS

In this section, four different theoretical calculations of the ^{12}C$(\gamma, p_{0+1})^{11}$B differential cross section by Ryckebusch *et al.* will be described and compared to the data

TABLE I. Differential cross sections in the c.m. frame for the reaction ^{12}C$(\gamma, p_{0+1})^{11}$B.

E_γ (MeV)	$d\sigma/d\Omega_{c.m.}$ (μb/sr)			
	$\theta_p^{c.m.} = 30.6°$	$\theta_p^{c.m.} = 45.8°$	$\theta_p^{c.m.} = 66.0°$	$\theta_p^{c.m.} = 91.1°$
44.1	—	66.6 ± 5.9	74.0 ± 4.3	41.2 ± 2.8
46.7	48.7 ± 7.0	59.7 ± 5.5	59.1 ± 3.8	35.8 ± 2.6
49.3	26.3 ± 5.2	51.3 ± 5.3	46.8 ± 3.6	27.1 ± 2.2
52.8	27.0 ± 5.5	37.7 ± 4.7	49.0 ± 3.7	16.3 ± 1.9
56.7	22.5 ± 3.6	33.2 ± 3.1	34.3 ± 2.2	11.6 ± 1.1
61.9	19.4 ± 3.5	21.9 ± 2.6	24.5 ± 2.0	8.5 ± 1.0
67.1	19.1 ± 3.8	21.4 ± 2.8	21.8 ± 2.0	5.3 ± 0.9
72.2	18.6 ± 3.9	13.1 ± 2.3	11.9 ± 1.6	3.0 ± 0.7
77.4	8.4 ± 2.6	12.8 ± 2.3	10.0 ± 1.5	1.6 ± 0.5
82.6	10.8 ± 3.1	11.5 ± 2.3	8.2 ± 1.4	2.1 ± 0.6
87.8	10.7 ± 3.2	11.4 ± 2.4	6.3 ± 1.3	1.7 ± 0.6
93.0	8.2 ± 2.9	5.2 ± 1.7	2.4 ± 0.8	0.6 ± 0.35
98.1	4.2 ± 2.1	5.3 ± 1.7	3.4 ± 0.9	0.2 ± 0.2

in Fig. 2. The calculations are similar to those previously reported [3,12], and can be categorized as follows:

(1) The first is a DKO calculation, using the one-body current form of the impulse approximation. A self-consistent Hartree-Fock formalism is used to calculate the bound-state wave functions and the phase shifts and partial waves of the ejected nucleon. Further details of this type of calculation can be found in Ref. [3]. Results from this calculation are displayed in Figs. 2 and 3 as the dotted lines.

(2) The second calculation is based on a DKO model similar to the first, except that the effects of MEC are included. The MEC are introduced by replacing the real nucleon mass by an effective mass in the convection current, as described in Ref. [3]. This effective mass is in principle a requirement for current conservation for the mean-field Hartree-Fock Hamiltonian generated by a Skyrme-type effective interaction. Results from this calculation will be referred to as DKO+MEC, and are displayed in Figs. 2 and 3 as the dot-dashed lines.

(3) In this calculation a random-phase-approximation (RPA) coupled-channel approach is taken, with the photoabsorption based on the one-body current of the impulse approximation. This model includes coupling to the collective properties of the target nucleus and rescattering effects, but no MEC are calculated. This calculation will be referred to as RPA, and its results are shown in Figs. 2 and 3 as the dashed lines.

(4) The fourth is an RPA coupled-channel calculation, with absorption based on the one-body current of the impulse approximation, plus two-body currents introduced using an effective Skyrme NN interaction. This NN interaction is used to generate the MEC and multistep processes, and all of the proton and neutron wave functions. MEC beyond the impulse approximation are generated by performing minimal substitution in the Skyrme effective NN Hamiltonian [24], preserving gauge invariance. A detailed description of this calculation has been given in Ref. [3]. It will be referred to as RPA+MEC, and its
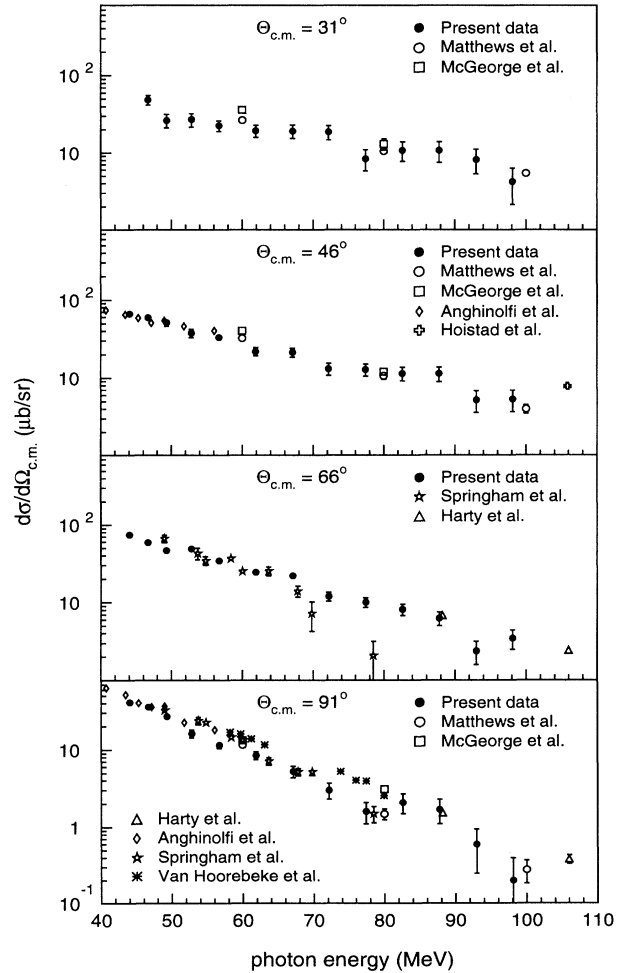

FIG. 1. Comparison of the present data with previous measurements of the ^{12}C$(\gamma, p_{0+1})^{11}$B differential cross section, as described in the text.

results are displayed in Figs. 2 and 3 as the solid lines.

There are some features common to all four of the calculations, which will be mentioned here. Each calculation starts with the one-body form of the impulse approximation, which has convection and magnetization currents added together. Each calculation assumes that the $\frac{3}{2}^{-}$ ground state and $\frac{1}{2}^{-}$ first excited state of ^{11}B are $1p_{3/2}$ and $1p_{1/2}$ holes, respectively. Spectroscopic factors for the calculations were obtained from an $(e,e'p)$ experiment by van der Steenhoven *et al.* [25]. These spectroscopic factors were 0.476 and 0.116 for the ground and first excited states, respectively. Last, distortions in the outgoing particle wave are accounted for in each calculation, but additional final-state interactions are calculated in both the RPA and RPA+MEC calculations, through rescattering effects.

It is clear from the comparison of data and theory in Fig. 2 that MEC have a dominant role in the photoabsorption process in this energy regime. In both the DKO
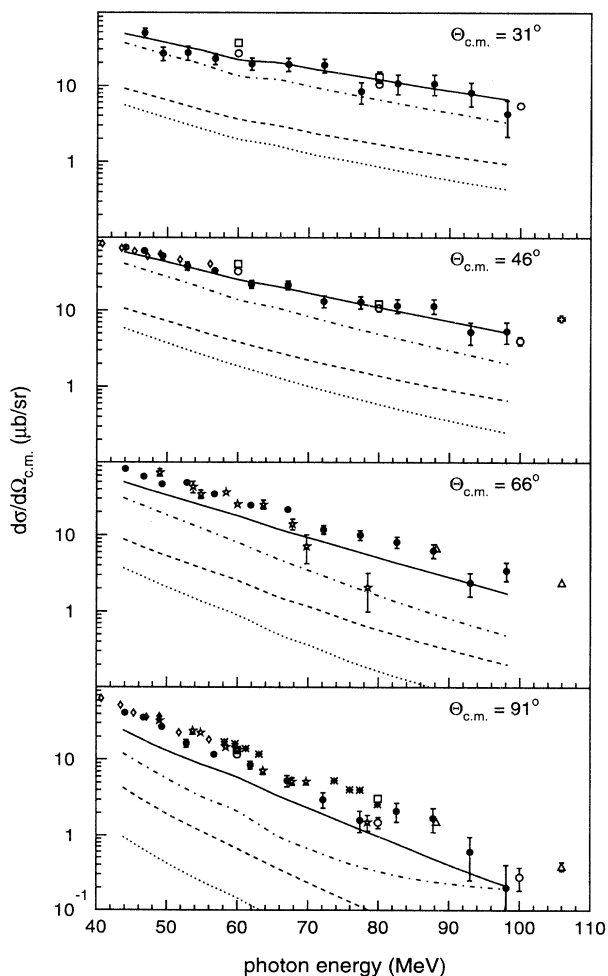

FIG. 3. Comparison of four theoretical calculations of the ^{12}C$(\gamma, n_0)^{11}$C differential cross section to previously published ^{12}C$(\gamma, n_{0+1})^{11}$C differential cross section data at $\theta_{c.m.} = 66°$ [7]. The theoretical curves are as in Fig. 2.

FIG. 2. Comparison of the measured ^{12}C$(\gamma, p_{0+1})^{11}$B differential cross section at four angles, with four theoretical calculations, DKO (dotted line), DKO+MEC (dot-dashed line), RPA (dashed line), and RPA+MEC (solid line). The data symbols are as in Fig. 1.
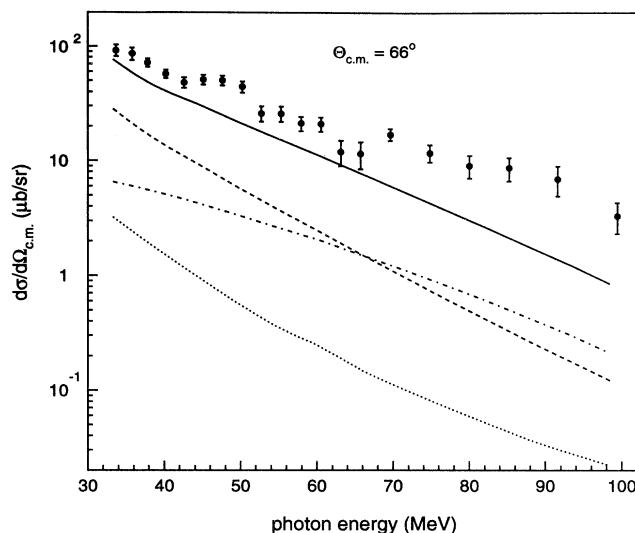
and RPA calculations there is an increase in cross section strength by an order of magnitude once MEC are added. It is also apparent that the best agreement is obtained with the RPA+MEC calculation.

An even greater disparity between the RPA+MEC and the other calculations is seen in Fig. 3 which shows a comparison of the calculated ^{12}C$(\gamma, n_0)^{11}$C differential cross section with previously published ^{12}C$(\gamma, n_{0+1})^{11}$C data at $\theta_{c.m.} = 66°$ [7]. In the absence of an experimental value for the spectroscopic factor, a value of 0.5 was used for the calculation of the ground-state cross section. The differential cross section leading to the first excited state in ^{11}C was not calculated, but is expected to be small compared to the ground-state cross section, as is the case for the photoproton channel. Comparing Figs. 2 and 3, it is clear that the DKO and DKO+MEC calculated results for ^{12}C$(\gamma, n_0)^{11}$C are much smaller than was calculated for the ^{12}C$(\gamma, p_{0+1})^{11}$B channel, and fail badly to reproduce the ^{12}C$(\gamma, n_{0+1})^{11}$C differential cross section data, especially at lower photon energies. The RPA and RPA+MEC results, however, are of comparable size to those calculated for ^{12}C$(\gamma, p_{0+1})^{11}$B, with the RPA+MEC calculation giving the best agreement with the data. At low photon energies, coupling to the collective properties of the target nucleus and rescattering effects are very important, and only the RPA and RPA+MEC calculations take these into account.

V. CONCLUSIONS

New data on the ^{12}C$(\gamma, p_{0+1})^{11}$B differential cross section have been presented, which cover a wide region of photon energies and four proton angles. Comparison has been made with four different calculations. In these comparisons it has been shown that the DKO reaction mecha-

nism fails to account for both the present ^{12}C$(\gamma, p_{0+1})^{11}$B data and the previously published ^{12}C$(\gamma, n_{0+1})^{11}$C data; however, the agreement with experiment is much improved when MEC are included. On the other hand, RPA calculations which include coupling to the collective properties of the target nucleus and rescattering effects, do much better in reproducing the data for both proton and neutron emission channels, especially when MEC are included.

Comparison between the calculations and data seem to indicate significant differences in the microscopic photo-absorption processes involved in the proton and neutron emission channels. It is seen that the dominant contribution to the differential cross section comes from the MEC in the case of the ^{12}C$(\gamma, p_{0+1})^{11}$B channel, and at ener-

gies greater than 70 MeV in the case of ^{12}C$(\gamma, n_0)^{11}$C. At lower photon energies, the ^{12}C$(\gamma, n_0)^{11}$C cross section is dominated by coupling to the collective properties of the target nucleus and rescattering effects. As pointed out in Ref. [3], the almost negligible contribution from DKO in the neutron emission channel is offset by a larger contribution from collective effects than in the proton channel, accounting for the overall similarity between n_0 and p_0 cross sections.

ACKNOWLEDGMENTS

[1] M. Gari and H. Hebach, Phys. Rep. **72**, 1 (1981); H. Hebach, A. Wortberg, and M. Gari, Nucl. Phys. **A267**, 425 (1976).

[2] M. Cavinato, M. Marangoni, P. L. Ottaviani, and A. M. Saruis, Nucl. Phys. **A373**, 445 (1982); M. Cavinato, M. Marangoni, and A. M. Saruis, Nuovo Cimento A **76**, 197 (1983); M. Cavinato, M. Marangoni, and A. M. Saruis, Nucl. Phys. **A422**, 237 (1984).

[3] J. Ryckebusch, M. Waroquier, K. Heyde, J. Moreau, and D. Ryckbosch, Nucl. Phys. **A476**, 237 (1988).

[4] S. Boffi, R. Cenni, C. Giusti, and F. D. Pacati, Nucl. Phys. **A420**, 38 (1984).

[5] B. Schoch, Phys. Rev. Lett. **41**, 80 (1978).

[6] J. S. Levinger, Phys. Rev. **84**, 43 (1951).

[7] P. D. Harty et al., Phys. Rev. C **37**, 13 (1988).

[8] E. J. Beise, G. Dodson, M. Garçon, S. Hoibråten, C. Maher, L. D. Pham, R. P. Redwine, W. Sapp, K. E. Wilson, and S. A. Wood, Phys. Rev. Lett. **62**, 2593 (1989).

[9] J. R. M. Annand, G. I. Crawford, P. D. Harty, J. C. McGeorge, G. J. Miller, B-E. Andersson, J-O. Adler, S. A. Bulychjev, L. Isaksson, H. Ruijter, and B. Schrøder, Phys. Rev. Lett. **71**, 2703 (1993).

[10] S. Cotanch and D. Robson, Nucl. Phys. **A209**, 301 (1973).

[11] J. T. Londergan and G. D. Nixon, Phys. Rev. C **19**, 998 (1979).

[12] J. Ryckebusch, K. Heyde, L. Machenil, D. Ryckbosch, M. Vanderhaeghen, and M. Waroquier, Phys. Rev. C **46**, R829 (1992).

[13] J. L. Matthews, D. J. S. Findlay, S. N. Gardiner, and R. O. Owens, Nucl. Phys. **A267**, 51 (1976).

[14] J. C. McGeorge et al., Phys. Lett. B **179**, 212 (1986).

[15] A. C. Shotter, S. Springham, D. Branford, J. Yorkston, J. C. McGeorge, B. Schoch, and P. Jennewein, Phys. Rev. C **37**, 1354 (1988).

[16] S. V. Springham et al., Nucl. Phys. **A517**, 93 (1990).

[17] L. Van Hoorebeke, Ph.D. thesis, University of Gent, Belgium, 1991; L. Van Hoorebeke et al., Phys. Rev. C **42**, R1179 (1990); L. Van Hoorebeke, D. Ryckbosch, R. Van de Vyver, F. De Smet, J-O. Adler, B-E. Andersson, L. Isaksson, A. Sandell, B. Schrøder, and K. Ziakas, ibid. **45**, 482 (1992).

[18] D. G. Ireland et al., Nucl. Phys. **A554**, 173 (1993).

[19] P. D. Harty et al., Phys. Rev. C **51**, 1982 (1995).

[20] M. Anghinolfi et al., Nucl. Phys. **A457**, 645 (1986).

[21] H. J. Hausman, S. L. Blatt, T. R. Donoghue, J. Kalen, W. Kim, D. G. Marchlenski, T. W. Rackers, P. Schmalbrook, M. A. Kovash, and A. D. Bacher, Phys. Rev. C **37**, 503 (1988).

[22] B. Höistad, E. Nilsson, J. Thun, S. Dahlgren, S. Isaksson, G. S. Adams, C. Landberg, T. B. Bright, and S. R. Cotanch, Phys. Lett. B **276**, 294 (1992).

[23] T. Terasawa et al., Nucl. Instrum. Methods **248**, 429 (1986).

[24] J. Ryckebusch, in Proceedings of the Workshop on Nuclear Physics with Real Photons below Pion Threshold, Gent, 1989 (unpublished), p. 19.

[25] G. van der Steenhoven, H. P. Blok, E. Jans, M. de Jong, L. Lapikas, E. N. M. Quint, and P. K. A. de Witt Huberts, Nucl. Phys. **A480**, 547 (1988); G. van der Steenhoven, H. P. Blok, E. Jans, L. Lapikas, E. N. M. Quint, and P. K. A. de Witt Huberts, ibid. **A484**, 445 (1988).